

## Polarization of $\Lambda$ ( $\bar{\Lambda}$ ) Hyperons along the Beam Direction in Au + Au Collisions at $\sqrt{s_{NN}} = 200$ GeV

J. Adam,<sup>13</sup> L. Adamczyk,<sup>2</sup> J. R. Adams,<sup>37</sup> J. K. Adkins,<sup>28</sup> G. Agakishiev,<sup>26</sup> M. M. Aggarwal,<sup>39</sup> Z. Ahammed,<sup>59</sup> I. Alekseev,<sup>3,33</sup> D. M. Anderson,<sup>53</sup> R. Aoyama,<sup>56</sup> A. Aparin,<sup>26</sup> D. Arkhipkin,<sup>6</sup> E. C. Aschenauer,<sup>6</sup> M. U. Ashraf,<sup>55</sup> F. Atetalla,<sup>27</sup> A. Attri,<sup>39</sup> G. S. Averichev,<sup>26</sup> V. Bairathi,<sup>34</sup> K. Barish,<sup>10</sup> A. J. Bassill,<sup>10</sup> A. Behera,<sup>51</sup> R. Bellwied,<sup>20</sup> A. Bhasin,<sup>25</sup> A. K. Bhati,<sup>39</sup> J. Bielcik,<sup>14</sup> J. Bielcikova,<sup>36</sup> L. C. Bland,<sup>6</sup> I. G. Bordyuzhin,<sup>3</sup> J. D. Brandenburg,<sup>48,6</sup> A. V. Brandin,<sup>33</sup> J. Bryslawskyj,<sup>10</sup> I. Bunzarov,<sup>26</sup> J. Butterworth,<sup>44</sup> H. Caines,<sup>62</sup> M. Calderón de la Barca Sánchez,<sup>8</sup> D. Cebra,<sup>8</sup> I. Chakaberia,<sup>27,6</sup> P. Chaloupka,<sup>14</sup> B. K. Chan,<sup>9</sup> F-H. Chang,<sup>35</sup> Z. Chang,<sup>6</sup> N. Chankova-Bunzarova,<sup>26</sup> A. Chatterjee,<sup>59</sup> S. Chattopadhyay,<sup>59</sup> J. H. Chen,<sup>18</sup> X. Chen,<sup>47</sup> J. Cheng,<sup>55</sup> M. Cherney,<sup>13</sup> W. Christie,<sup>6</sup> H. J. Crawford,<sup>7</sup> M. Csanád,<sup>16</sup> S. Das,<sup>11</sup> T. G. Dedovich,<sup>26</sup> I. M. Deppner,<sup>19</sup> A. A. Derevschikov,<sup>41</sup> L. Didenko,<sup>6</sup> C. Dilks,<sup>40</sup> X. Dong,<sup>29</sup> J. L. Drachenberg,<sup>1</sup> J. C. Dunlop,<sup>6</sup> T. Edmonds,<sup>42</sup> N. Elsey,<sup>61</sup> J. Engelage,<sup>7</sup> G. Eppley,<sup>44</sup> R. Esha,<sup>51</sup> S. Esumi,<sup>56</sup> O. Evdokimov,<sup>12</sup> J. Ewigleben,<sup>30</sup> O. Eyser,<sup>6</sup> R. Fatemi,<sup>28</sup> S. Fazio,<sup>6</sup> P. Federic,<sup>36</sup> J. Fedorisin,<sup>26</sup> Y. Feng,<sup>42</sup> P. Filip,<sup>26</sup> E. Finch,<sup>50</sup> Y. Fisyak,<sup>6</sup> L. Fulek,<sup>2</sup> C. A. Gagliardi,<sup>53</sup> T. Galatyuk,<sup>15</sup> F. Geurts,<sup>44</sup> A. Gibson,<sup>58</sup> K. Gopal,<sup>22</sup> D. Grosnick,<sup>58</sup> A. Gupta,<sup>25</sup> W. Guryn,<sup>6</sup> A. I. Hamad,<sup>27</sup> A. Hamed,<sup>5</sup> J. W. Harris,<sup>62</sup> L. He,<sup>42</sup> S. Heppelmann,<sup>8</sup> S. Heppelmann,<sup>40</sup> N. Herrmann,<sup>19</sup> L. Holub,<sup>14</sup> Y. Hong,<sup>29</sup> S. Horvat,<sup>62</sup> B. Huang,<sup>12</sup> H. Z. Huang,<sup>9</sup> S. L. Huang,<sup>51</sup> T. Huang,<sup>35</sup> X. Huang,<sup>55</sup> T. J. Humanic,<sup>37</sup> P. Huo,<sup>51</sup> G. Igo,<sup>9</sup> W. W. Jacobs,<sup>23</sup> C. Jena,<sup>22</sup> A. Jentsch,<sup>54</sup> Y. Ji,<sup>47</sup> J. Jia,<sup>6,51</sup> K. Jiang,<sup>47</sup> S. Jowzaee,<sup>61</sup> X. Ju,<sup>47</sup> E. G. Judd,<sup>7</sup> S. Kabana,<sup>27</sup> S. Kagamaster,<sup>30</sup> D. Kalinkin,<sup>23</sup> K. Kang,<sup>55</sup> D. Kapukchyan,<sup>10</sup> K. Kauder,<sup>6</sup> H. W. Ke,<sup>6</sup> D. Keane,<sup>27</sup> A. Kechechyan,<sup>26</sup> M. Kelsey,<sup>29</sup> Y. V. Khyzhniak,<sup>33</sup> D. P. Kikoła,<sup>60</sup> C. Kim,<sup>10</sup> T. A. Kinghorn,<sup>8</sup> I. Kisel,<sup>17</sup> A. Kisel,<sup>60</sup> M. Kocan,<sup>14</sup> L. Kochenda,<sup>33</sup> L. K. Kosarzewski,<sup>14</sup> L. Kramerik,<sup>14</sup> P. Kravtsov,<sup>33</sup> K. Krueger,<sup>4</sup> N. Kulathunga Mudiyansele,<sup>20</sup> L. Kumar,<sup>39</sup> R. Kunnawalkam Elayavalli,<sup>61</sup> J. H. Kwasizur,<sup>23</sup> R. Lacey,<sup>51</sup> J. M. Landgraf,<sup>6</sup> J. Lauret,<sup>6</sup> A. Lebedev,<sup>6</sup> R. Lednicky,<sup>26</sup> J. H. Lee,<sup>6</sup> C. Li,<sup>47</sup> W. Li,<sup>49</sup> W. Li,<sup>44</sup> X. Li,<sup>47</sup> Y. Li,<sup>55</sup> Y. Liang,<sup>27</sup> R. Licenik,<sup>14</sup> T. Lin,<sup>53</sup> A. Lipiec,<sup>60</sup> M. A. Lisa,<sup>37</sup> F. Liu,<sup>11</sup> H. Liu,<sup>23</sup> P. Liu,<sup>51</sup> P. Liu,<sup>49</sup> T. Liu,<sup>62</sup> X. Liu,<sup>37</sup> Y. Liu,<sup>53</sup> Z. Liu,<sup>47</sup> T. Ljubicic,<sup>6</sup> W. J. Llope,<sup>61</sup> M. Lomnitz,<sup>29</sup> R. S. Longacre,<sup>6</sup> S. Luo,<sup>12</sup> X. Luo,<sup>11</sup> G. L. Ma,<sup>49</sup> L. Ma,<sup>18</sup> R. Ma,<sup>6</sup> Y. G. Ma,<sup>49</sup> N. Magdy Abdelwahab Abdelrahman,<sup>12</sup> R. Majka,<sup>62</sup> D. Mallick,<sup>34</sup> S. Margetis,<sup>27</sup> C. Markert,<sup>54</sup> H. S. Matis,<sup>29</sup> O. Matonoha,<sup>14</sup> J. A. Mazer,<sup>45</sup> K. Meehan,<sup>8</sup> J. C. Mei,<sup>48</sup> N. G. Minaev,<sup>41</sup> S. Mioduszewski,<sup>53</sup> D. Mishra,<sup>34</sup> B. Mohanty,<sup>34</sup> M. M. Mondal,<sup>24</sup> I. Mooney,<sup>61</sup> Z. Moravcova,<sup>14</sup> D. A. Morozov,<sup>41</sup> Md. Nasim,<sup>9</sup> K. Nayak,<sup>11</sup> J. M. Nelson,<sup>7</sup> D. B. Nemes,<sup>62</sup> M. Nie,<sup>48</sup> G. Nigmatkulov,<sup>33</sup> T. Niida,<sup>56,61</sup> L. V. Nogach,<sup>41</sup> T. Nonaka,<sup>11</sup> G. Odyniec,<sup>29</sup> A. Ogawa,<sup>6</sup> K. Oh,<sup>43</sup> S. Oh,<sup>62</sup> V. A. Okorokov,<sup>33</sup> B. S. Page,<sup>6</sup> R. Pak,<sup>6</sup> Y. Panebratsev,<sup>26</sup> B. Pawlik,<sup>38</sup> D. Pawłowska,<sup>60</sup> H. Pei,<sup>11</sup> C. Perkins,<sup>7</sup> R. L. Pintér,<sup>16</sup> J. Pluta,<sup>60</sup> J. Porter,<sup>29</sup> M. Posik,<sup>52</sup> N. K. Pruthi,<sup>39</sup> M. Przybycien,<sup>2</sup> J. Putschke,<sup>61</sup> A. Quintero,<sup>52</sup> S. K. Radhakrishnan,<sup>29</sup> S. Ramachandran,<sup>28</sup> R. L. Ray,<sup>54</sup> R. Reed,<sup>30</sup> H. G. Ritter,<sup>29</sup> J. B. Roberts,<sup>44</sup> O. V. Rogachevskiy,<sup>26</sup> J. L. Romero,<sup>8</sup> L. Ruan,<sup>6</sup> J. Rusnak,<sup>36</sup> O. Rusnakova,<sup>14</sup> N. R. Sahoo,<sup>48</sup> P. K. Sahu,<sup>24</sup> S. Salur,<sup>45</sup> J. Sandweiss,<sup>62</sup> J. Schambach,<sup>54</sup> W. B. Schmidke,<sup>6</sup> N. Schmitz,<sup>31</sup> B. R. Schweid,<sup>51</sup> F. Seck,<sup>15</sup> J. Seger,<sup>13</sup> M. Sergeeva,<sup>9</sup> R. Seto,<sup>10</sup> P. Seyboth,<sup>31</sup> N. Shah,<sup>49</sup> E. Shahaliev,<sup>26</sup> P. V. Shanmuganathan,<sup>30</sup> M. Shao,<sup>47</sup> F. Shen,<sup>48</sup> W. Q. Shen,<sup>49</sup> S. S. Shi,<sup>11</sup> Q. Y. Shou,<sup>49</sup> E. P. Sichtermann,<sup>29</sup> S. Siejka,<sup>60</sup> R. Sikora,<sup>2</sup> M. Simko,<sup>36</sup> J. Singh,<sup>39</sup> S. Singha,<sup>27</sup> D. Smirnov,<sup>6</sup> N. Smirnov,<sup>62</sup> W. Solyst,<sup>23</sup> P. Sorensen,<sup>6</sup> H. M. Spinka,<sup>4</sup> B. Srivastava,<sup>42</sup> T. D. S. Stanislaus,<sup>58</sup> M. Stefaniak,<sup>60</sup> D. J. Stewart,<sup>62</sup> M. Strikhanov,<sup>33</sup> B. Stringfellow,<sup>42</sup> A. A. P. Suaide,<sup>46</sup> T. Sugiura,<sup>56</sup> M. Sumera,<sup>36</sup> B. Summa,<sup>40</sup> X. M. Sun,<sup>11</sup> Y. Sun,<sup>47</sup> Y. Sun,<sup>21</sup> B. Surrow,<sup>52</sup> D. N. Svirida,<sup>3</sup> P. Szymanski,<sup>60</sup> A. H. Tang,<sup>6</sup> Z. Tang,<sup>47</sup> A. Taranenko,<sup>33</sup> T. Tarnowsky,<sup>32</sup> J. H. Thomas,<sup>29</sup> A. R. Timmins,<sup>20</sup> D. Tlusty,<sup>13</sup> T. Todoroki,<sup>6</sup> M. Tokarev,<sup>26</sup> C. A. Tomkiel,<sup>30</sup> S. Trentalange,<sup>9</sup> R. E. Tribble,<sup>53</sup> P. Tribedy,<sup>6</sup> S. K. Tripathy,<sup>24</sup> O. D. Tsai,<sup>9</sup> B. Tu,<sup>11</sup> Z. Tu,<sup>6</sup> T. Ullrich,<sup>6</sup> D. G. Underwood,<sup>4</sup> I. Upsal,<sup>48,6</sup> G. Van Buren,<sup>6</sup> J. Vanek,<sup>36</sup> A. N. Vasiliev,<sup>41</sup> I. Vassiliev,<sup>17</sup> F. Videbæk,<sup>6</sup> S. Vokal,<sup>26</sup> S. A. Voloshin,<sup>61</sup> F. Wang,<sup>42</sup> G. Wang,<sup>9</sup> P. Wang,<sup>47</sup> Y. Wang,<sup>11</sup> Y. Wang,<sup>55</sup> J. C. Webb,<sup>6</sup> L. Wen,<sup>9</sup> G. D. Westfall,<sup>32</sup> H. Wieman,<sup>29</sup> S. W. Wissink,<sup>23</sup> R. Witt,<sup>57</sup> Y. Wu,<sup>27</sup> Z. G. Xiao,<sup>55</sup> G. Xie,<sup>12</sup> W. Xie,<sup>42</sup> H. Xu,<sup>21</sup> N. Xu,<sup>29</sup> Q. H. Xu,<sup>48</sup> Y. F. Xu,<sup>49</sup> Z. Xu,<sup>6</sup> C. Yang,<sup>48</sup> Q. Yang,<sup>48</sup> S. Yang,<sup>6</sup> Y. Yang,<sup>35</sup> Z. Yang,<sup>11</sup> Z. Ye,<sup>44</sup> Z. Ye,<sup>12</sup> L. Yi,<sup>48</sup> K. Yip,<sup>6</sup> I.-K. Yoo,<sup>43</sup> H. Zbroszczyk,<sup>60</sup> W. Zha,<sup>47</sup> D. Zhang,<sup>11</sup> L. Zhang,<sup>11</sup> S. Zhang,<sup>47</sup> S. Zhang,<sup>49</sup> X. P. Zhang,<sup>55</sup> Y. Zhang,<sup>47</sup> Z. Zhang,<sup>49</sup> J. Zhao,<sup>42</sup> C. Zhong,<sup>49</sup> C. Zhou,<sup>49</sup> X. Zhu,<sup>55</sup> Z. Zhu,<sup>48</sup> M. Zurek,<sup>29</sup> and M. Zyzak<sup>17</sup>

(STAR Collaboration)

<sup>1</sup>Abilene Christian University, Abilene, Texas 79699<sup>2</sup>AGH University of Science and Technology, FPACS, Cracow 30-059, Poland

- <sup>3</sup>*Alikhanov Institute for Theoretical and Experimental Physics, Moscow 117218, Russia*
- <sup>4</sup>*Argonne National Laboratory, Argonne, Illinois 60439*
- <sup>5</sup>*American Univerisity of Cairo, New Cairo 11835, Egypt*
- <sup>6</sup>*Brookhaven National Laboratory, Upton, New York 11973*
- <sup>7</sup>*University of California, Berkeley, California 94720*
- <sup>8</sup>*University of California, Davis, California 95616*
- <sup>9</sup>*University of California, Los Angeles, California 90095*
- <sup>10</sup>*University of California, Riverside, California 92521*
- <sup>11</sup>*Central China Normal University, Wuhan, Hubei 430079*
- <sup>12</sup>*University of Illinois at Chicago, Chicago, Illinois 60607*
- <sup>13</sup>*Creighton University, Omaha, Nebraska 68178*
- <sup>14</sup>*Czech Technical University in Prague, FNSPE, Prague 115 19, Czech Republic*
- <sup>15</sup>*Technische Universität Darmstadt, Darmstadt 64289, Germany*
- <sup>16</sup>*Eötvös Loránd University, Budapest, Hungary H-1117*
- <sup>17</sup>*Frankfurt Institute for Advanced Studies FIAS, Frankfurt 60438, Germany*
- <sup>18</sup>*Fudan University, Shanghai 200433*
- <sup>19</sup>*University of Heidelberg, Heidelberg 69120, Germany*
- <sup>20</sup>*University of Houston, Houston, Texas 77204*
- <sup>21</sup>*Huzhou University, Huzhou, Zhejiang 313000*
- <sup>22</sup>*Indian Institute of Science Education and Research, Tirupati 517507, India*
- <sup>23</sup>*Indiana University, Bloomington, Indiana 47408*
- <sup>24</sup>*Institute of Physics, Bhubaneswar 751005, India*
- <sup>25</sup>*University of Jammu, Jammu 180001, India*
- <sup>26</sup>*Joint Institute for Nuclear Research, Dubna 141 980, Russia*
- <sup>27</sup>*Kent State University, Kent, Ohio 44242*
- <sup>28</sup>*University of Kentucky, Lexington, Kentucky 40506-0055*
- <sup>29</sup>*Lawrence Berkeley National Laboratory, Berkeley, California 94720*
- <sup>30</sup>*Lehigh University, Bethlehem, Pennsylvania 18015*
- <sup>31</sup>*Max-Planck-Institut für Physik, Munich 80805, Germany*
- <sup>32</sup>*Michigan State University, East Lansing, Michigan 48824*
- <sup>33</sup>*National Research Nuclear University MEPhI, Moscow 115409, Russia*
- <sup>34</sup>*National Institute of Science Education and Research, HBNI, Jatni 752050, India*
- <sup>35</sup>*National Cheng Kung University, Tainan 70101*
- <sup>36</sup>*Nuclear Physics Institute of the CAS, Rez 250 68, Czech Republic*
- <sup>37</sup>*Ohio State University, Columbus, Ohio 43210*
- <sup>38</sup>*Institute of Nuclear Physics PAN, Cracow 31-342, Poland*
- <sup>39</sup>*Panjab University, Chandigarh 160014, India*
- <sup>40</sup>*Pennsylvania State University, University Park, Pennsylvania 16802*
- <sup>41</sup>*NRC “Kurchatov Institute,” Institute of High Energy Physics, Protvino 142281, Russia*
- <sup>42</sup>*Purdue University, West Lafayette, Indiana 47907*
- <sup>43</sup>*Pusan National University, Pusan 46241, Korea*
- <sup>44</sup>*Rice University, Houston, Texas 77251*
- <sup>45</sup>*Rutgers University, Piscataway, New Jersey 08854*
- <sup>46</sup>*Universidade de São Paulo, São Paulo, Brazil 05314-970*
- <sup>47</sup>*University of Science and Technology of China, Hefei, Anhui 230026*
- <sup>48</sup>*Shandong University, Qingdao, Shandong 266237*
- <sup>49</sup>*Shanghai Institute of Applied Physics, Chinese Academy of Sciences, Shanghai 201800*
- <sup>50</sup>*Southern Connecticut State University, New Haven, Connecticut 06515*
- <sup>51</sup>*State University of New York, Stony Brook, New York 11794*
- <sup>52</sup>*Temple University, Philadelphia, Pennsylvania 19122*
- <sup>53</sup>*Texas A&M University, College Station, Texas 77843*
- <sup>54</sup>*University of Texas, Austin, Texas 78712*
- <sup>55</sup>*Tsinghua University, Beijing 100084*
- <sup>56</sup>*University of Tsukuba, Tsukuba, Ibaraki 305-8571, Japan*
- <sup>57</sup>*United States Naval Academy, Annapolis, Maryland 21402*
- <sup>58</sup>*Valparaiso University, Valparaiso, Indiana 46383*
- <sup>59</sup>*Variable Energy Cyclotron Centre, Kolkata 700064, India*
- <sup>60</sup>*Warsaw University of Technology, Warsaw 00-661, Poland*
- <sup>61</sup>*Wayne State University, Detroit, Michigan 48201*
- <sup>62</sup>*Yale University, New Haven, Connecticut 06520*

 (Received 28 May 2019; revised manuscript received 21 August 2019; published 27 September 2019)

The  $\Lambda$  ( $\bar{\Lambda}$ ) hyperon polarization along the beam direction has been measured in Au + Au collisions at  $\sqrt{s_{NN}} = 200$  GeV, for the first time in heavy-ion collisions. The polarization dependence on the hyperons' emission angle relative to the elliptic flow plane exhibits a second harmonic sine modulation, indicating a quadrupole pattern of the vorticity component along the beam direction, expected due to elliptic flow. The polarization is found to increase in more peripheral collisions, and shows no strong transverse momentum ( $p_T$ ) dependence at  $p_T$  greater than 1 GeV/ $c$ . The magnitude of the signal is about 5 times smaller than those predicted by hydrodynamic and multiphase transport models; the observed phase of the emission angle dependence is also opposite to these model predictions. In contrast, the kinematic vorticity calculations in the blast-wave model tuned to reproduce particle spectra, elliptic flow, and the azimuthal dependence of the Gaussian source radii measured with the Hanbury Brown–Twiss intensity interferometry technique reproduce well the modulation phase measured in the data and capture the centrality and transverse momentum dependence of the polarization signal.

DOI: [10.1103/PhysRevLett.123.132301](https://doi.org/10.1103/PhysRevLett.123.132301)

The properties of deconfined partonic matter, the quark-gluon plasma, have been explored in heavy-ion collisions at the Relativistic Heavy Ion Collider (RHIC) [1–4] and the Large Hadron Collider [5–7]. The matter created in non-central heavy-ion collisions should exhibit rotational motion in order to conserve the initial angular momentum carried by the two colliding nuclei. The direction of the angular momentum is perpendicular to the reaction plane, as defined by the incoming beam and the impact parameter vector. It was predicted [8,9] that such a spinning motion of the matter would lead to a net spin polarization of particles produced in the collisions due to spin-orbit coupling. Hyperons are natural candidates to explore this phenomenon since in the parity violating weak decays of the hyperons the momentum vector of the decay baryon is highly correlated with the hyperon spin. In such decays the angular distribution of the daughter baryons is given by

$$\frac{dN}{d\cos\theta^*} \propto 1 + \alpha_H P_H \cos\theta^*, \quad (1)$$

where  $\alpha_H$  is the hyperon decay parameter ( $\alpha_\Lambda = -\alpha_{\bar{\Lambda}} = 0.642 \pm 0.013$  for  $\Lambda$  and  $\bar{\Lambda}$ ) [10,11],  $P_H$  is the hyperon polarization, and  $\theta^*$  is the angle between the polarization vector and the direction of the daughter baryon momentum in the hyperon rest frame.

The Solenoidal Tracker at RHIC (STAR) Collaboration has observed positive polarizations of  $\Lambda$  hyperons along the orbital angular momentum in Au + Au collisions for collision energies of  $\sqrt{s_{NN}} = 7.7$ –200 GeV [14,15]. This polarization is evidence for the creation of the most vortical fluid ever observed, with vorticities of the order of  $\omega \sim 10^{22}$  s $^{-1}$ . These results open new opportunities for a better understanding of the dynamics and properties of the matter created in heavy-ion collisions.

The spin polarization of hyperons along the orbital angular momentum of the entire system is referred to as the global polarization, meaning a net spin alignment along a specific direction uniquely determined in a collision.

However, the vorticity and, consequently, the particle polarization may vary for different regions of the fluid due to anisotropic flow, energy deposits from jet quenching, density fluctuations, etc. The detailed structure of the vorticity fields may be complicated and the resulting particle polarization can depend on the particle transverse momentum and the azimuthal angle relative to the reaction plane, or even exhibit toroidal structures [16–19].

Anisotropic flow, characterized by the Fourier coefficients of the particle azimuthal distribution in the transverse plane, has been extensively studied in heavy-ion collisions and was found to be well described by hydrodynamic calculations [20,21]. Nontrivial velocity fields describing transverse anisotropic flow should lead to a vorticity component along the beam direction dependent on the azimuthal angle relative to the reaction plane [17,18]. The observation of the large second-order coefficients, also known as elliptic flow, in midcentral collisions indicates significantly stronger expansion in the reaction plane direction compared to that out of plane, which might lead to a quadrupole structure in the  $z$  component of vorticity, as illustrated in Fig. 1. Experimental measurements of such a component are the main goal of this analysis.

The beam direction component of the polarization arising from vorticity due to elliptic flow is expected to be more sensitive to the later stages of the system evolution following the anisotropic flow development [22] than the global polarization that originates mostly from the initial velocity fields. It might also have different sensitivity to the relaxation time needed for the conversion of the vorticity into particle polarization. Therefore, measurements of the particle polarization along the beam direction in heavy-ion collisions are of great interest for further understanding of the vorticity dynamics in heavy-ion collisions and its relation to the polarization. In this Letter, we report the beam direction component of polarization for  $\Lambda$  and  $\bar{\Lambda}$  hyperons in Au + Au collisions at  $\sqrt{s_{NN}} = 200$  GeV. The results are presented as functions of the collision centrality and the hyperons' transverse momentum ( $p_T$ ).

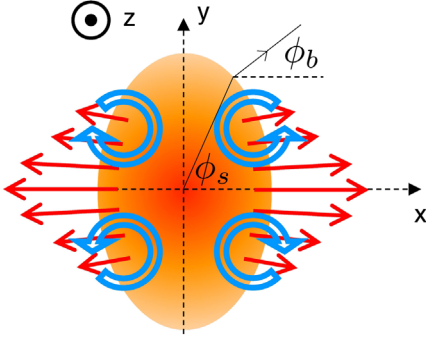


FIG. 1. A sketch illustrating the system created in a noncentral heavy-ion collision viewed in the transverse plane ( $x$ - $y$ ), showing stronger in-plane expansion (solid arrows) and expected vorticities (open arrows). Here, the colliding beams are oriented along the  $z$  axis and the  $x$ - $z$  plane defines the reaction plane. See text for explanations of  $\phi_s$  and  $\phi_b$ .

The dataset for this analysis was collected in 2014 by the STAR detector during the period of Au + Au collisions at  $\sqrt{s_{NN}} = 200$  GeV. Charged-particle tracks were measured in the time projection chamber (TPC) [23], which covers the full azimuth and a pseudorapidity range of  $-1 < \eta < 1$ . The collision vertices were reconstructed using the measured charged-particle tracks. Events were selected to have the collision vertex position within 6 cm of the center of the TPC in the beam direction and within 2 cm in the radial direction with respect to the beam center. In addition, the difference between the vertex positions along the beam direction determined by the TPC and the vertex position detectors (VPD) [24] located at forward and backward rapidities ( $4.24 < |\eta| < 5.1$ ) was required to be less than 3 cm to suppress pileup events. These selection criteria yielded about  $1 \times 10^9$  minimum bias events, where the minimum bias trigger required hits of both VPDs and the zero-degree calorimeters [25] located at  $|\eta| > 6.3$ .

The collision centrality was determined from the measured multiplicity of charged particles within  $|\eta| < 0.5$  and a Monte Carlo Glauber simulation [26]. The second-order event plane ( $\Psi_2$ ) as an experimental estimate of the reaction plane was determined by the charged-particle tracks within the transverse momentum range of  $0.15 < p_T < 2$  GeV/ $c$  and  $0.1 < |\eta| < 1$  in the same way as in Ref. [27]. The resolution of the measured plane  $\Psi_2^{\text{obs}}$  defined as  $\text{Res}(\Psi_2) = \langle \cos 2(\Psi_2^{\text{obs}} - \Psi_2) \rangle$  was estimated with the two-subevent method [28], where the two subevents correspond to pseudorapidity regions  $-1 < \eta < -0.1$  and  $0.1 < \eta < 1$ . In midcentral collisions the event plane resolution peaks at  $\sim 0.76$ .

Charged particles of good quality TPC tracks (see Ref. [15] for details) with  $0.15 < p_T < 10$  GeV/ $c$  and  $|\eta| < 1$  were used in this analysis.  $\Lambda$  and  $\bar{\Lambda}$  hyperons were reconstructed via decay channels  $\Lambda \rightarrow p + \pi^-$  and  $\bar{\Lambda} \rightarrow \bar{p} + \pi^+$ , corresponding to  $(63.9 \pm 0.5)\%$  of all decays [10]]. The hyperon identification was based on the invariant

mass of the two daughters with cuts on decay topology to reduce the combinatoric background [15].

The component of the polarization along the beam direction  $P_z$  can be measured by taking  $\theta_p^*$  in Eq. (1) as the polar angle of the daughter proton in the  $\Lambda$  ( $\bar{\Lambda}$ ) rest frame and calculating the  $\langle \cos \theta_p^* \rangle$ . This yields

$$P_z = \frac{\langle \cos \theta_p^* \rangle}{\alpha_H \langle \cos^2 \theta_p^* \rangle}. \quad (2)$$

The factor  $\langle \cos^2 \theta_p^* \rangle$ , expected to be  $\sim 1/3$  for the case of the perfect detector acceptance, was extracted from the data to account for finite pseudorapidity acceptance. It was found to be close to  $1/3$  at all collision centralities, but showed a systematic decrease at low  $p_T$ .

A significant fraction of  $\Lambda$  and  $\bar{\Lambda}$  are the decay products of heavier baryons such as  $\Sigma^*$  and  $\Xi$ . This leads to about  $\sim 10\%$  reduction in measured  $\Lambda$  polarization compared to that of primary  $\Lambda$  [29,30]. No correction for feed-down effects are done in the current analysis.

To extract the signal  $\langle \cos \theta_p^* \rangle$ , two techniques were used: the event plane method and the invariant mass method. In the event plane method,  $\langle \cos \theta_p^* \rangle$  was measured as a function of azimuthal angle of  $\Lambda$  ( $\bar{\Lambda}$ ) relative to  $\Psi_2$ . The effects due to detector acceptance and inefficiencies are removed by requiring that the azimuthal average to be zero, as expected due to symmetry. Figure 2 shows  $\langle \cos \theta_p^* \rangle^{\text{sub}}$  of  $\Lambda$  and  $\bar{\Lambda}$  as a function of azimuthal angle relative to  $\Psi_2$  for the 20%–60% centrality bin. The solid lines indicate the fit results to the function  $p_0 + 2p_1 \sin(2\phi - 2\Psi_2)$ , where  $p_0$

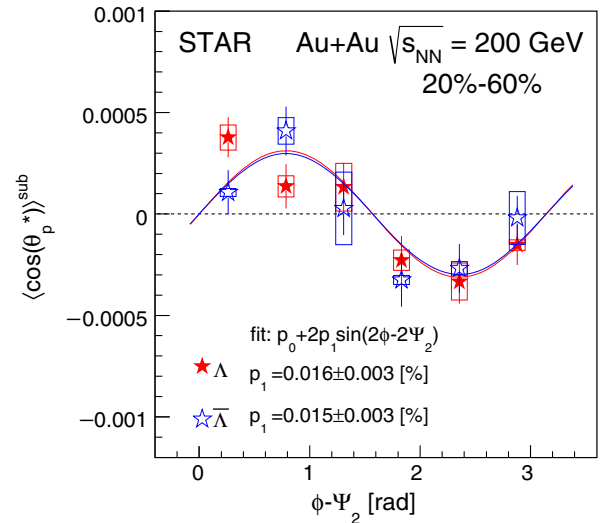


FIG. 2.  $\langle \cos \theta_p^* \rangle$  of  $\Lambda$  and  $\bar{\Lambda}$  hyperons as a function of azimuthal angle  $\phi$  relative to the second-order event plane  $\Psi_2$  for 20%–60% centrality bin in Au + Au collisions at  $\sqrt{s_{NN}} = 200$  GeV. Open boxes show the systematic uncertainties and  $\langle \rangle^{\text{sub}}$  denotes the subtraction of the acceptance effect (see text). Solid lines show the fit with the sine function shown inside the figure. Note that the data are not corrected for the event plane resolution.

and  $p_1$  are fit parameters. The data are consistent with a sine structure for both  $\Lambda$  and  $\bar{\Lambda}$ , as expected from the elliptic flow.

In the invariant mass method, the second-order Fourier sine coefficient of  $P_z$ ,  $p_1 = \langle P_z \sin(2\phi - 2\Psi_2) \rangle$ , was measured as a function of the invariant mass. Following the same procedure as described in Ref. [15], the sine coefficient was directly extracted. The extracted coefficients in both methods were divided by  $\text{Res}(\Psi_2)$  to account for the finite event plane resolution. The invariant mass method was used to calculate the sine coefficient of  $P_z$  reported below and the event plane method was used to cross-check and provide an estimate of the systematic uncertainty.

The systematic uncertainties were estimated by variation of the topological cuts ( $< 2\%$ ), comparing the results from two methods for signal extraction (5%) as mentioned above, using different subevents ( $-1 < \eta < -0.5$  and  $0.5 < \eta < 1$ ) for  $\Psi_2$  determination ( $< 11\%$ ), and estimates of the possible background contribution to the signal (4.3%). The numbers are for midcentral collisions. Also the uncertainty from the decay parameter is accounted for (2% for  $\Lambda$  and 9.6% for  $\bar{\Lambda}$ ; see Ref. [15] for details). We further studied the effect of a possible self-correlation between the particles used for the  $\Lambda$  ( $\bar{\Lambda}$ ) reconstruction and the event plane by explicitly removing the daughter particles from the event plane calculation. There was no significant difference between the results. The  $\Lambda$  and  $\bar{\Lambda}$  reconstruction efficiencies were estimated using GEANT [31] simulations of the STAR detector [23]. The correction is found to lower mean values of the  $P_z$  sine coefficient by  $\sim 10\%$  in peripheral collisions and increases up to  $\sim 50\%$  in central collisions, although the variations are within statistical uncertainties. No significant difference was observed between  $\Lambda$  and  $\bar{\Lambda}$  as expected. Therefore, results from both samples were combined to reduce statistical uncertainties.

Figure 3 presents the centrality dependence of the second Fourier sine coefficient  $\langle P_z \sin(2\phi - 2\Psi_2) \rangle$ . The increase of the signal with decreasing centrality is likely due to increasing elliptic flow contributions in peripheral collisions. We note that, unlike elliptic flow, the polarization seems to disappear in the most central collisions, where the elliptic flow is still significant due to initial density fluctuations. Because of large uncertainties in peripheral collisions, it is not clear whether the signal continues to increase or levels off. The results are compared to a multiphase transport (AMPT) model [32]. The AMPT model predicts the opposite phase of the modulations and overestimates the magnitude.

Since the elliptic flow also depends on  $p_T$  as well as on the centrality, the polarization may have  $p_T$  dependence. Figure 4 shows the sine coefficients of  $P_z$  as a function of the hyperon transverse momentum. No significant  $p_T$  dependence is observed for  $p_T > 1$  GeV/c, and the statistical precision of the single data point for  $p_T < 1$  GeV/c is not enough to allow for definitive conclusions about the

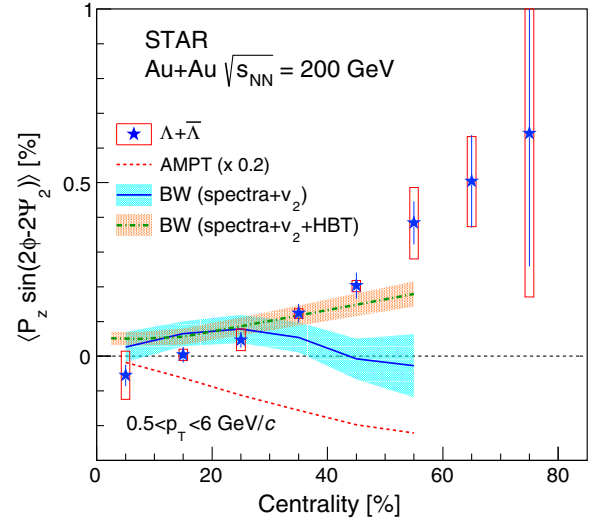


FIG. 3. The second Fourier sine coefficient of the polarization of  $\Lambda$  and  $\bar{\Lambda}$  along the beam direction as a function of the collision centrality in Au + Au collisions at  $\sqrt{s_{NN}} = 200$  GeV. Open boxes show the systematic uncertainties. Dotted line shows the AMPT calculation [32] scaled by 0.2 (no  $p_T$  selection). Solid and dot-dashed lines with the bands show the blast-wave (BW) model calculation for  $p_T = 1$  GeV/c with  $\Lambda$  mass (see text for details).

low  $p_T$  dependence. In the hydrodynamic model calculation [18], the sine coefficient of  $P_z$  increases in magnitude with  $p_T$  but shows the opposite sign to the data.

The reason for this sign difference between the data and the model calculations is under discussion [33–35]. It is likely related to the relative contributions to the polarization from the kinematic vorticity originating from the elliptic flow, and from the temporal gradient of temperatures at the time of hadronization [18]. A recent calculation using the chiral kinetic approach predicts the same sign as the data [36]. The model accounts for the transverse component of the vorticity, resulting in the axial charge currents. Both the hydrodynamic and transport models calculate local vorticity at freeze-out and convert it to the polarization assuming local thermal equilibrium of the spin degrees of freedom, while the chiral kinetic approach takes into account nonequilibrium effects but does not consider a contribution from the temperature gradient, which is a main source of  $P_z$  in the hydrodynamic model.

Both the hydrodynamic and chiral kinetic models indicate that the contribution from the kinematic vorticity to  $P_z$  is negligible or opposite in sign to the naive expectation from the elliptic flow. In order to estimate the contribution from the kinematic vorticity, we employed the boost invariant blast-wave (BW) model [37–39]. Following Ref. [39], the system transverse velocity field at freeze-out can be parametrized with temperature ( $T$ ) and transverse flow rapidity ( $\rho$ ) defined as  $\rho = \tilde{r}[\rho_0 + \rho_2 \cos(2\phi_b)]$ . Here  $\rho_0$  and  $\rho_2$  are the maximal radial expansion rapidity and its azimuthal modulation,  $\tilde{r}$  is the relative distance to the edge of the source, and  $\phi_b$  defines the direction of the

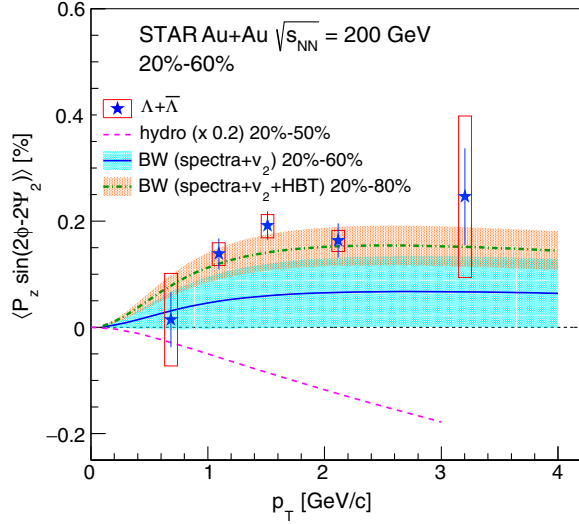


FIG. 4. The second Fourier sine coefficient of the longitudinal polarization of  $\Lambda$  and  $\bar{\Lambda}$  hyperons as a function of  $p_T$  for 20%–60% centrality bin in Au + Au collisions at  $\sqrt{s_{NN}} = 200$  GeV. Open boxes show the systematic uncertainties. Magenta dashed line shows the hydrodynamic model calculation [18] scaled by 0.2. Solid and dot-dashed lines with the bands show the blast-wave model calculations with  $\Lambda$  mass.

local velocity as indicated in Fig. 1. The source shape, assumed to be elliptical in the transverse plane, is parametrized by the  $R_y$  and  $R_x$  radii. To obtain the BW parameters, two fits are performed: in one only spectra and elliptic flow of  $\pi$ ,  $K$ , and  $p(\bar{p})$  are fit; the second fit also includes azimuthal-angle dependence of the pion Gaussian source radii at freeze-out as measured via Hanbury Brown–Twiss (HBT) intensity interferometry (see Ref. [40]).

The average longitudinal vorticity can be calculated in a similar way to the elliptic flow:

$$\langle \omega_z \sin(2\phi) \rangle = \frac{\int d\phi_s \int r dr I_2(\alpha_t) K_1(\beta_t) \omega_z \sin(2\phi_b)}{\int d\phi_s \int r dr I_0(\alpha_t) K_1(\beta_t)}, \quad (3)$$

$$\omega_z = \frac{1}{2} \left( \frac{\partial u_y}{\partial x} - \frac{\partial u_x}{\partial y} \right), \quad (4)$$

where the integration is over the transverse cross-sectional area of the source,  $u_\mu$  is a four-vector of the local flow velocity [39],  $\phi_s$  is the azimuth of the production point (see Fig. 1 for the relation to  $\phi_b$ ),  $\alpha_t = p_T/T \sinh \rho$ ,  $\beta_t = m_T/T \cosh \rho$ , and  $I_n$  and  $K_1$  are the modified Bessel functions. Assuming a local thermal equilibrium, the longitudinal component of the polarization can be predicted as  $P_z \approx \omega_z/(2T)$ . The uncertainties shown for the BW model calculations correspond to  $1\sigma$  variation in the model parameters.

In Figs. 3 and 4 the BW calculations are compared to the data. From central to midcentral collisions both BW calculations show positive sine coefficients which are

compatible in both sign and magnitude to the measurement, although the BW model is based on a very simple picture of the freeze-out condition. It was shown in Ref. [17] that the vorticity in the BW model has the effects of the velocity field anisotropy ( $\rho_2/\rho_0$ ) and the spacial source anisotropy ( $R_y/R_x$ ) contributing with opposite signs, which can explain a strong sensitivity of the BW model predictions in the peripheral collisions to the inclusions of the HBT radii.

In summary, we have presented the first measurements of the longitudinal component of the polarization for  $\Lambda$  and  $\bar{\Lambda}$  hyperons in Au + Au collisions at  $\sqrt{s_{NN}} = 200$  GeV. A quadrupole modulation of the polarization along the beam direction is observed and found to be qualitatively consistent with the expectation from the vorticity component along the beam direction due to the elliptic flow. The results exhibit a strong centrality dependence with increasing magnitude as the collision centrality becomes more peripheral. No significant  $p_T$  dependence is observed above  $p_T > 1$  GeV/c. A dropoff of the signal is hinted at for  $p_T < 1$  GeV/c. Disagreement in the polarization sign between the data and hydrodynamic and AMPT models might indicate incomplete thermal equilibration of the spin degrees of freedom for the beam direction component of the vorticity or polarization, as it develops later in time compared to the global polarization. On the other hand, the blast-wave model calculations are much closer to the data, even more so when the azimuthally sensitive HBT results along with the  $p_T$  spectra and  $v_2$  are included in the model fit. The blast-wave model predicts the correct phase of  $P_z$  modulation and a similar  $p_T$  dependence; the version with HBT radii included in the fit also reasonably describes the centrality dependence. These results together with the results of the global polarization may provide information on the relaxation time needed to convert the vorticity to particle polarization. Further theoretical and experimental studies are needed for better understanding.

We thank the RHIC Operations Group and RCF at BNL, the NERSC Center at LBNL, and the Open Science Grid consortium for providing resources and support. This work was supported in part by the Office of Nuclear Physics within the U.S. DOE Office of Science, the U.S. National Science Foundation, the Ministry of Education and Science of the Russian Federation, National Natural Science Foundation of China, Chinese Academy of Science, the Ministry of Science and Technology of China and the Chinese Ministry of Education, the National Research Foundation of Korea, Czech Science Foundation and Ministry of Education, Youth and Sports of the Czech Republic, Hungarian National Research, Development and Innovation Office, New National Excellency Programme of the Hungarian Ministry of Human Capacities, Department of Atomic Energy and Department of Science and Technology of the Government of India, the National Science Centre of Poland, the Ministry of Science,

Education and Sports of the Republic of Croatia, RosAtom of Russia and German Bundesministerium für Bildung, Wissenschaft, Forschung und Technologie (BMBF) and the Helmholtz Association.

- 
- [1] J. Adams *et al.* (STAR Collaboration), Experimental and theoretical challenges in the search for the quark gluon plasma: The STAR Collaboration's Critical Assessment of the evidence from RHIC collisions, *Nucl. Phys.* **A757**, 102 (2005).
- [2] K. Adcox *et al.* (PHENIX Collaboration), Formation of dense partonic matter in relativistic nucleus-nucleus collisions at RHIC: Experimental evaluation by the PHENIX Collaboration, *Nucl. Phys.* **A757**, 184 (2005).
- [3] B. B. Back *et al.* (PHOBOS Collaboration), The PHOBOS perspective on discoveries at RHIC, *Nucl. Phys.* **A757**, 28 (2005).
- [4] I. Arsene *et al.* (BRAHMS Collaboration), Quark gluon plasma and color glass condensate at RHIC? The perspective from the BRAHMS experiment, *Nucl. Phys.* **A757**, 1 (2005).
- [5] K. Aamodt *et al.* (ALICE Collaboration), Suppression of charged particle production at large transverse momentum in central Pb-Pb collisions at  $\sqrt{s_{NN}} = 2.76$  TeV, *Phys. Lett. B* **696**, 30 (2011).
- [6] S. Chatrchyan *et al.* (CMS Collaboration), Observation and studies of jet quenching in PbPb collisions at  $\sqrt{s_{NN}} = 2.76$  TeV, *Phys. Rev. C* **84**, 024906 (2011).
- [7] G. Aad *et al.* (ATLAS Collaboration), Observation of a Centrality-Dependent Dijet Asymmetry in Lead-Lead Collisions at  $\sqrt{s_{NN}} = 2.76$  TeV with the ATLAS Detector at the LHC, *Phys. Rev. Lett.* **105**, 252303 (2010).
- [8] Z. T. Liang and X. N. Wang, Globally Polarized Quark-Gluon Plasma in Noncentral A + A Collisions, *Phys. Rev. Lett.* **94**, 102301 (2005); Erratum, *Phys. Rev. Lett.* **96**, 039901 (2006).
- [9] S. A. Voloshin, Polarized secondary particles in unpolarized high energy hadron-hadron collisions?, [arXiv:nucl-th/0410089](https://arxiv.org/abs/nucl-th/0410089).
- [10] C. Patrignani *et al.* (Particle Data Group), Review of particle physics, *Chin. Phys. C* **40**, 100001 (2016).
- [11] Recent studies [12,13] show 12%–17% higher  $\alpha_\Lambda$  than Ref. [10]. Therefore, the measured polarization could be smaller by that amount.
- [12] M. Ablikim *et al.* (BESIII Collaboration), Polarization and entanglement in baryon-antibaryon pair production in electron-positron annihilation, *Nat. Phys.* **15**, 631 (2019).
- [13] D. G. Ireland, M. Dring, D. I. Glazier, J. Haidenbauer, M. Mai, R. Murray-Smith, and D. Rönchen, Kaon photoproduction and the  $\Lambda$  decay parameter  $\alpha_\Lambda$ , [arXiv:1904.07616](https://arxiv.org/abs/1904.07616).
- [14] L. Adamczyk *et al.* (STAR Collaboration), Global  $\Lambda$  hyperon polarization in nuclear collisions, *Nature (London)* **548**, 62 (2017).
- [15] J. Adam *et al.* (STAR Collaboration), Global polarization of  $\Lambda$  hyperons in Au + Au collisions at  $\sqrt{s_{NN}} = 200$  GeV, *Phys. Rev. C* **98**, 014910 (2018).
- [16] B. Betz, M. Gyulassy, and G. Torrieri, Polarization probes of vorticity in heavy ion collisions, *Phys. Rev. C* **76**, 044901 (2007).
- [17] S. A. Voloshin, Vorticity and particle polarization in heavy ion collisions (experimental perspective), *EPJ Web Conf.* **171**, 07002 (2018).
- [18] F. Becattini and Iu. Karpenko, Collective Longitudinal Polarization in Relativistic Heavy-Ion Collisions at Very High Energy, *Phys. Rev. Lett.* **120**, 012302 (2018).
- [19] L.-G. Pang, H. Petersen, Q. Wang, and X.-N. Wang, Vortical Fluid and  $\Lambda$  Spin Correlations in High-Energy Heavy-Ion Collisions, *Phys. Rev. Lett.* **117**, 192301 (2016).
- [20] S. A. Voloshin, A. M. Poskanzer, and R. Snellings, *Collective Phenomena in Non-Central Nuclear Collisions*, Landolt-Bornstein, vol. 23 (Springer-Verlag, Berlin, Heidelberg, 2010), p. 293.
- [21] U. Heinz and R. Snellings, Collective flow and viscosity in relativistic heavy-ion collisions, *Annu. Rev. Nucl. Part. Sci.* **63**, 123 (2013).
- [22] D. Teaney and L. Yan, Triangularity and dipole asymmetry in relativistic heavy ion collisions, *Phys. Rev. C* **83**, 064904 (2011).
- [23] M. Anderson *et al.*, The STAR time projection chamber: A unique tool for studying high multiplicity events at RHIC, *Nucl. Instrum. Methods Phys. Res., Sect. A* **499**, 659 (2003).
- [24] W. J. Llope *et al.*, The STAR vertex position detector, *Nucl. Instrum. Methods Phys. Res., Sect. A* **759**, 23 (2014).
- [25] C. Adler, A. Denisov, E. Garcia, M. Murray, H. Strobele, and S. White, The RHIC zero degree calorimeters, *Nucl. Instrum. Methods Phys. Res., Sect. A* **461**, 337 (2001).
- [26] L. Adamczyk *et al.* (STAR Collaboration), Inclusive charged hadron elliptic flow in Au + Au collisions at  $\sqrt{s_{NN}} = 7.7$ –39 GeV, *Phys. Rev. C* **86**, 054908 (2012).
- [27] L. Adamczyk *et al.* (STAR Collaboration), Elliptic flow of identified hadrons in Au + Au collisions at  $\sqrt{s_{NN}} = 7.7$ –62.4 GeV, *Phys. Rev. C* **88**, 014902 (2013).
- [28] A. M. Poskanzer and S. A. Voloshin, Methods for analyzing anisotropic flow in relativistic nuclear collisions, *Phys. Rev. C* **58**, 1671 (1998).
- [29] X.-L. Xia, H. Li, X.-G. Huang, and H. Z. Huang, Feed-down effect on  $\Lambda$  spin polarization, *Phys. Rev. C* **100**, 014913 (2019).
- [30] F. Becattini, G. Cao, and E. Speranza, Polarization transfer in hyperon decays and its effect in relativistic nuclear collisions, [arXiv:1905.03123](https://arxiv.org/abs/1905.03123).
- [31] R. Brun, F. Bruyant, M. Maire, A. C. McPherson, and P. Zanarini, GEANT 3: User's guide Geant 3.10, Geant 3.11 (CERN, Geneva 1987).
- [32] X.-L. Xia, H. Li, Z.-B. Tang, and Q. Wang, Probing vorticity structure in heavy-ion collisions by local  $\Lambda$  polarization, *Phys. Rev. C* **98**, 024905 (2018).
- [33] W. Florkowski, A. Kumar, R. Ryblewski, and A. Mazeliauskas, Longitudinal spin polarization in a thermal model, [arXiv:1904.00002](https://arxiv.org/abs/1904.00002).
- [34] Y. Xie, D. Wang, and L. P. Csernai, Fluid dynamics study of the  $\Lambda$  polarization for Au+Au collisions at  $\sqrt{s_{NN}} = 200$  GeV, [arXiv:1907.00773](https://arxiv.org/abs/1907.00773).

- [35] H.-Z. Wu, L.-G. Pang, X.-G. Huang, and W. Qun, Local spin polarization in high energy heavy ion collisions, [arXiv:1906.09385](#).
- [36] Y. Sun and C. M. Ko, Azimuthal angle dependence of the longitudinal spin polarization in relativistic heavy ion collisions, *Phys. Rev. C* **99**, 011903(R) (2019).
- [37] E. Schnedermann, J. Sollfrank, and U. W. Heinz, Thermal phenomenology of hadrons from 200 A GeV S + S collisions, *Phys. Rev. C* **48**, 2462 (1993).
- [38] C. Adler *et al.* (STAR Collaboration), Identified Particle Elliptic Flow in Au + Au Collisions at  $\sqrt{s_{NN}} = 130$  GeV, *Phys. Rev. Lett.* **87**, 182301 (2001).
- [39] F. Retiere and M. A. Lisa, Observable implications of geometrical and dynamical aspects of freeze-out in heavy ion collisions, *Phys. Rev. C* **70**, 044907 (2004).
- [40] J. Adams *et al.* (STAR Collaboration), Pion interferometry in Au + Au collisions at  $\sqrt{s_{NN}} = 200$  GeV, *Phys. Rev. C* **71**, 044906 (2005).